PLOS ONE

RESEARCH ARTICLE

Probabilistic behavioral aggregation: A case study on the Nordic power grid

Anna Büttner, Frank Hellmann*

Complexity Science, Potsdam-Institute for Climate Impact Research, Potsdam, Germany

* hellmann@pik-potsdam.de

Check for updates

OPEN ACCESS

Citation: Büttner A, Hellmann F (2025) Probabilistic behavioral aggregation: A case study on the Nordic power grid. PLoS One 20(8): e0322328. https://doi.org/10.1371/journal.pone.0322328

Editor: Tiago Pereira, Universidade de Sao Paulo, BRAZIL

Received: November 05, 2024

Accepted: March 19, 2025

Published: August 25, 2025

Copyright: © 2025 Büttner, Hellmann. This is an open access article distributed under the terms of the Creative Commons Attribution License, which permits unrestricted use, distribution, and reproduction in any medium, provided the original author and source are credited.

Data availability statement: All files are available from the Zenodo database (accession number https://doi.org/10.5281/zenodo.14040008).

Funding: None of the funders played any role in the study design, data collection and analysis, decision to publish, or preparation of the manuscript. A. Büttner, German Academic Scholarship Foundation, PhD Scholarship, No Grant Number, https://www.studienstiftung.de/. A. Büttner, DFG - Deutsche

Abstract

This study applies the Probabilistic Behavioral Tuning (ProBeTune) framework to transient power grid simulations to address challenges posed by increasing grid complexity. ProBeTune offers a probabilistic approach to model aggregation, using a behavioral distance measure to quantify and minimize discrepancies between a full-scale system and a simplified model. We demonstrate the effectiveness of ProBeTune on the Nordic5 (N5) test case, a model representing the Nordic power grid with complex nodal dynamics and a high share of RESs. We substantially reduce the complexity of the dynamics by tuning the system to align with a reduced swing-equation model. We confirm the validity of the swing equation with tailored controllers and parameter distributions for capturing the essential dynamics of the Nordic region. This reduction could allow interconnected systems like the Central European power grid to treat the Nordic grid as a single dynamic actor, facilitating more manageable stability assessments. The findings lay the groundwork for future research on applying ProBeTune to microgrids and other complex sub-systems, aiming to enhance scalability and accuracy in power grid modeling amidst rising complexity.

1 Introduction

Transient simulations of power grids form the foundation of dynamic stability assessment tools [1]. These tools are integral to control room operations, enabling transmission system operators to predict and mitigate critical grid states. For instance, the European Network of Transmission System Operators (ENTSO-E) mandates the simulation of large fault scenario sets to enhance the stability assessment of power grids [2,3]. However, the feasibility of these approaches remains constrained by the substantial computational demands of transient simulations.

As renewable energy sources (RESs) increasingly replace synchronous generation, the number of grid actors rises, given that each RES typically produces less energy than a traditional power plant. This shift introduces profound challenges: RESs inherently lack inertia—a fundamental element of stability in conventional grids [4]. Additionally, they promote decentralized grid structures [5] and exhibit volatile production patterns [6]. These changes collectively transform grid dynamics, increasing complexity.

Forschungsgemeinschaft, Grant Number: KU 837/39-2, https://www.dfg.de/. A. Büttner, BMWK - Federal Ministry for Economic Affairs and Climate Action, Grant Number: 03EI1016A, https://www.bmwk.de/Navigation/DE/Home/home.html.

Competing interests: The authors have declared that no competing interests exist.

A system with exponentially more dynamic components demands significantly greater computational resources for dynamic analysis. Consequently, managing the complexity of future power systems is essential for enabling dynamic stability assessments and ensuring the secure operation of power grids.

Model order reduction techniques, such as balanced truncation, are commonly used to simplify parts of power systems [7]. Transient simulations can be sped up significantly by replacing sub-systems with simpler models. However, ensuring that the reduced model reliably represents the entire system is challenging due to the non-linear and networked nature of power grids. This uncertainty can be problematic: if the reduced sub-system does not accurately reflect the entire system's behavior during transient simulations, it might trigger false alarms when the system is stable or, worse, overlook critical states. Therefore, it is crucial to quantify the accuracy of reduced models.

Recently, the "Probabilistic Behavioral Tuning" (ProBeTune) framework was introduced to address this issue [8]. ProBeTune provides probabilistic distance measures to specify the distance between reduced and full models. Realistic power grids face many possible scenarios where the system is perturbed from its stable operation. The probabilistic approach allows us to explicitly model the scenarios and quantify how well the reduced model represents the full model under these scenarios.

In this paper, we apply ProBeTune to the Nordic5 (N5) test case, a model representing the Nordic power grid, which is characterized by complex nodal dynamics and a high share of renewable energy sources (RES) [9]. This study aims to simplify the dynamics of the Nordic region to a single swing equation at the grid connection point to the Central European (CE) system. The swing equation with a range of permissible parameters specifies the aggregate behavior. Such specifications are well suited to encode the stabilizing behavior of the aggregate subsystem towards the overall system. Achieving this aggregation would allow the CE system to treat the Nordic region as a single, simplified actor, thereby reducing complexity.

ProBeTune is introduced in detail in Sect 2.2. Information on the modeling of the N5 can be found in Sect 2.1. The different control designs and scenarios examined in this work are detailed in Sects 2.3.1 and 2.4, respectively. We compare the performance of ProBeTune to an analytic baseline, which we introduce in Sect 3.1. The main findings of our study are detailed in Sect 3, where we demonstrate that the aggregated behavior of the N5 system can be tuned to behave like a swing equation. This shows that sophisticated grids, subject to unknown disturbances, can be tuned to simple specifications. The results presented in this paper lay the groundwork for future research aimed at aggregating and optimizing the dynamics of power grids using fully differentiable models.

2 Methods

2.1 Nordic5

The Nordic5 (N5) test case was introduced in [9] and is an ideal candidate for studying with ProBeTune, as it exhibits intriguing dynamic phenomena. The network structure of the N5 and the desired specification are illustrated in Fig 1. The N5 is densely coupled internally but has only a single connection to Central Europe (CE). Each bus in the N5 features a load and at least one energy source, as indicated in the figure. A third-order machine models the CE bus [10,11], with an additional load at the bus.

Each bus in the N5 system contains a rotor whose frequency dynamics are described by the classical swing equation model. The swing equation represents the equation of motion for the rotor, accounting for mechanical, electrical, and inertial torques, and captures the short-term

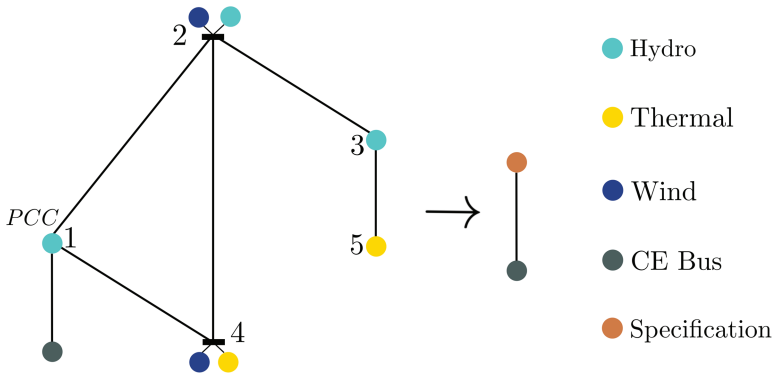


Fig 1. Network structure of the N5 system. Each bus consists of a load, a controller, and additional energy sources. Bus 1 connects the N5 to central Europe via a high-voltage direct current (HVDC) link. The goal is to reduce the entire N5 system to the specification shown in orange.

https://doi.org/10.1371/journal.pone.0322328.g001

behavior of a machine's rotor. The model is widely utilized in electrical engineering [12] and is also known in the theoretical physics literature as the second-order Kuramoto model [13].

We have added proportional control $D_i\omega_i$ to each rotor as the baseline form of control. This results in the following frequency dynamics ω_i for bus i:

$$\dot{\omega}_i = \frac{1}{2H_i}\left(P_{m,i} - P_{e,i} - D_i\omega_i\right) \tag{1}$$

where H_i is the inertia constant, $P_{m,i}$, and $P_{e,i}$ are the mechanical and electrical power, respectively, that are given by the corresponding differential equations of the machine models, governors, and exciters.

Following [9], the thermal machines are modeled as sixth-order machines, with an IEEE Type 1 voltage regulator as the exciter, a fourth-order controller as the power system stabilizer (PSS), and a rotor. The hydro machines are represented by a fifth-order machine model, a rotor, and a simplified version of the non-linear governor model introduced in [14]. The block diagrams depicting these models are provided in S1–S3 Figs in S1 Appendix.

The governor's power production initially undershoots when the reference power P_{ref} is increased [15], which could lead to dangerously low frequencies and the triggering of cascading failures. To overcome this issue, the authors of [9] have equipped the governor with a frequency containment reserve (FCR) controller. The different FCR-control designs are introduced in Sect 2.3.1. The wind turbines are described by the model introduced in [16] that includes a grid-following inverter and an additional FCR controller.

2.2 Probabilistic behavioral distances

This section will introduce the "Probabilistic Behavioral Tuning" (ProBeTune) framework, a probabilistic aggregation technique based on a behavioral approach.

The behavioral approach defines systems by their behaviors, the sets of inputs, and respective outputs that arise in response to these inputs. This approach focuses on the observable behavior of the system rather than its internal structure. By defining systems through their behaviors, we can directly compare the dynamic response of different systems. This is particularly useful when dealing with complex, interconnected systems such as power grids. The article [17] provides an excellent introduction to the behavioral approach for dynamical

systems. Power grids are subject to various sources of uncertainty, such as fluctuating demand, variable renewable energy supply, and unexpected disturbances. A probabilistic approach allows us to model and account for these complex uncertainties explicitly.

In [8], the authors introduce the concept of probabilistic distance measures for non-linear systems with stochastic inputs. This distance measures how far the behavior of a system is from the behavior of an idealized, reduced specification. The specification is defined as a set of desirable, simple dynamical equations parameterized by a set of parameters q.

For the N5 system, the specification is chosen as the swing equation, representing the idealized behavior in response to a power imbalance. Being close to this idealized behavior indicates that the internal complexities have been effectively hidden from the central European system. Using ProBeTune, we aim to optimize the *controllable* parameters p of the N5 system so that its dynamics closely resemble those described by a single swing equation. In Sect 2.3.1, we describe which parameters are fixed and controllable.

For the N5 system, as seen from the CE grid, a natural choice for the output is the frequency $\omega(t)$ visible at the connection point between the grids. For the N5 system, the input from the CE grid is the current flowing on the transmission line between them. The output metric o is based on the L_2-norm between the frequency of the system at the Point of Common Coupling (PCC), ω_{pcc}, and the frequency of the specification, ω_{spec}. The output metric is this L_2 norm averaged over all scenarios N and includes possibly scenario-dependent specification parameters q_k:

$$o(p,q) = \frac{1}{N}\sum_{k=1}^{N}\sum_{t}\left(|\omega_{pcc}^{k}(p,t) - \omega_{\text{spec}}^{k}(q_k,t)|\right)^2, \tag{2}$$

where k and t run over the N scenarios and 5000 uniformly distributed time points in the time series, respectively. This metric requires an ensemble of scenarios sampled from a probability distribution ρ. It is crucial to choose these ensembles carefully, as the distances can only be guaranteed for the probability distribution from which the ensembles have been drawn. The considered scenarios are discussed in Sect 2.4.

The behavioral distance, as defined in [8], is given by the minimum of the output metric (2) with respect to q:

$$d^{\rho} = \min_{q} o(p,q), \tag{3}$$

which means that *only* the parameters of the specification are optimized. This distance can be used to validate how close the system and specification are at different steps of the tuning pipeline. We refer to the distance before any additional N5 parameters p tuning as the initial distance d^{ρ}_{init}.

In a second step, the controllable parameters p of the N5 and the specification q are optimized *jointly* such that $\omega_{pcc}(t)$ and $\omega_{spec}(t)$ come as close to each other as possible. To find the set of optimal parameters (p_{opt}, q_{opt}), the authors of [8] formulate a joint-optimization problem:

$$(p_{opt}, q_{opt}) = \arg\min_{p}\min_{q} o(p,q). \tag{4}$$

With this optimal set of parameters, the behavioral distance after tuning d^{ρ}_{end} is calculated to validate how close the system and specification are. To verify that no over-fitting occurred, N new samples are drawn, and the resampled behavioral distance d^{ρ}_{re} is estimated. If

the distance d^{ρ}_{re} does not increase significantly from d^{ρ}_{end}, we can be sure that the specification does not only memorize the training samples but adequately represents the system behavior. Hence, we can be confident that the specification accurately captures the dynamic behavior of the N5. All steps of the tuning pipeline are summarized in Table 1.

The approach has been implemented numerically as calculating the behavioral distance and the optimal parameters is typically analytically intractable. In principle, traditional optimization techniques, such as grid search, can be used to calculate the distance and determine the optimal parameters. However, the resulting computation times are unfeasible for practical applications. To perform these optimizations within reasonable times, gradient-descent methods and auto-differentiation are required. In the literature, ProBeTune has not been applied to realistic power grids, only to conceptual oscillator networks [8], due to the lack of a fully differentiable power grid model. A major contribution of this work is demonstrating that building and optimizing a fully differentiable complex grid model is feasible. In the S1 Appendix, we highlight the software and computational methods we have employed to achieve such a fully differentiable system.

Recently, several papers have been published that address the aggregation of behaviors to achieve desirable dynamics. Among them is [9], which introduced the N5 test case. Particularly noteworthy are the publications by Häberle et al. [18,19], which aim to achieve desired multi-input multi-output behavior. The authors achieve each device's desired global and local behavior and focus on providing ancillary services. In contrast, our focus is on aggregation and thus only specifies a global specification. Notably, in [18], only linear parameter-varying systems, a class of non-linear systems that can be expressed as linear systems with state-dependent parameters, can be considered the specification. Our approach, however, allows for utilizing fully non-linear specifications. This is desirable as non-linearities characterize the dynamics of power grids and must be included in an appropriate reduced model for transient simulations.

2.3 Specification

In the following, we introduce the specification employed, a single swing equation with controlled power generation, as the reduced model for the N5. The dynamics for the modified swing equation with controlled power generation is given by:

$$\begin{aligned} \dot{\omega} &= \frac{1}{2H}\left(P_{ref} - P_e - D\omega\right) \\ P_{ref} &= P_{fix} + u(\omega) \end{aligned} \tag{5}$$

where $u(\omega)$ is the control input and P_{fix} is the power consumption of the load in the operation point.

Table 1. Steps of the tuning pipeline used in this paper.

Tuning Pipeline Steps
Draw N random samples from ρ
Calculate baseline o_{base}
Estimate the initial distance d^{ρ}_{init}
Tune system and specification to each other
Estimate d^{ρ}_{end} after tuning
Draw N new samples and calculate d^{ρ}_{re}

https://doi.org/10.1371/journal.pone.0322328.t001

The swing equation can be understood as the idealized behavior of a power plant or region to a power imbalance. Being close to this idealized dynamic behavior means that the CE system can treat the Nordic region as the simpler model that facilitates dynamic simulations. We use the same control input u in the specification and before the governors in the N5. In addition to the control parameters, we also allow the inertia constant H of the specification to be tuned.

2.3.1 Controllers. In this section, we introduce the tunable controllers in the N5, especially the FCR controllers employed by the hydro-governor and wind turbines. We have fixed all model parameters of the N5 to the values given in the literature [9] except those of the FCR controller and the proportional control, which we assumed to be adaptable. These parameters are optimized to tune the N5 to behave as the specification. In particular, the inertia constants H_i of the machines are fixed, as they are determined by the design of the rotating components. A summary of the controllers and the controllable parameters for the system p and specification q is provided in Table 2 at the end of the section.

We employ proportional control at the rotor as the baseline and progress towards more elaborate control schemes, such as leaky integral controllers [20]. Using only proportional control results in a deviation between the asymptotic and nominal frequency when the power is changed. This deviation arises from the power mismatch that cannot be counterbalanced, resulting in undesirable behavior. Despite this, proportional control remains of interest as the swing equation with a proportional term is analytically well understood [21].

The FCR-controller, which has been included in the model to prevent undershoots, measures the local frequency and calculates the reference power P_{ref} as follows:

$$P_{ref,i} = P_{fix,i} + u_i(\omega_i) \tag{6}$$

where $P_{fix,i}$ is the power bus i generates in the operation point and u_i is the control input of the FCR-controller at bus i. The additional FCR control aims to adjust the power production of all generators to restore power balance and achieve the nominal frequency ω_0.

First, we added integral control to the FCR controller given in Eq (6), which is given by the following control input:

$$u_i = -K_i \int \omega_i dt, \tag{7}$$

where K_i is the integral gain at bus i. We call the combination of proportional and integral controllers PI-controllers, which aligns with the traditional literature.

Additionally, we have implemented leaky integral control, which was introduced in [20]. The leaky integral controller is a fully decentralized frequency restoration controller. The authors of [20] have shown that the leaky integral controller accomplishes a trade-off between performance and robustness and between asymptotic disturbance rejection and transient convergence rate by tuning the control parameters. The control input u_i of the leaky integral

Table 2. Summary of the tuneable parameters for the system and the specification.

Controller	Parameters System	Parameters Specification
P (no additional FCR-Control)	D_i	D,H
PI	D_i, K_i	D,K,H
PLI	D_i, G_i, T_i	D,G,T,H

https://doi.org/10.1371/journal.pone.0322328.t002

controller at bus i is given by:

$$u_i = -y_i \tag{8}$$

$$\frac{dy_i}{dt} = \frac{1}{T_i}(\omega_i - G_i y_i). \tag{9}$$

where T_i and K_i are the time and gain constant at bus i respectively. The leaky integral controller, in combination with a proportional term, is referred to as a PLI controller.

2.4 Scenarios

The probabilistic distances introduced above require an ensemble of scenarios. It is crucial to choose these ensembles carefully as the distances obtained can only be guaranteed for the probability distribution ρ the scenarios have been drawn from. In the following, we consider two different models for demand fluctuations: one paradigmatic and the other more realistic. In addition to demand fluctuations, the approach can also incorporate production fluctuations, such as those from wind [22] or solar energy [23], as stochastic processes for these sources are well-established. This could be explored in future publications.

The demand of the CE bus is given by $P_d = P_{load} + P_{fluc}(t)$, where P_{load} is the power the bus consumes in the steady state and $P_{fluc}(t)$ is the fluctuation.

First, we consider a random Fourier model, similar to that used in [8], to induce a complex response in the system. This model is based on smooth random functions, which provide a convenient framework for exploring random effects while enabling the use of numerical methods for ordinary differential equations, avoiding the need for algorithms designed for stochastic differential equations. Further details on this methodology can be found in the review article [24]. The resulting demand fluctuation is generated by combining modes with random amplitudes A_n and phase shifts ϕ_n, as described by the following equation:

$$P_{fluc}(t) = \sum_{n=1}^{N_{freq}} A_n \cos(t \cdot n + \phi_n). \tag{10}$$

We always use $N_{freq} = 10$ different modes in this example. Fig 2 shows two possible realizations of this process.

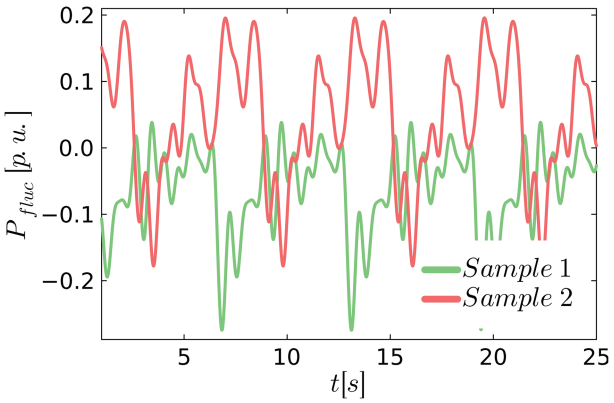


Fig 2. Two realizations of the random modes.

https://doi.org/10.1371/journal.pone.0322328.g002

Second, we also use a proper stochastic process for demand fluctuations, given in Eq 12, using the model introduced in [25], which provides a more realistic picture. The authors of the study propose a methodology for extracting both the average demand profiles $P_{trend}(t)$ and the demand fluctuations $P_{fluc}(t)$ from demand time series data. They introduce a stochastic model to capture real-world demand fluctuations that are asymmetric and heavy-tailed. In this work, we only focus on the fluctuation as we only study short-term dynamics. To describe the fluctuations, Ornstein-Uhlenbeck processes are used:

$$dx_i(t) = -\gamma x_i(t)dt + \epsilon dW_i \tag{11}$$

where γ is the damping coefficient, ϵ is the noise amplitude of the Wiener processes W. These processes are used to define the power fluctuation $P_{fluc}(t)$:

$$P_{fluc}(t) = \sqrt{\sum_{i=1}^{J} x_i(t)^2} + \mu_{MB} \tag{12}$$

where μ_{MB} is the observed shift from zero and J is the number of independent Ornstein-Uhlenbeck processes. As suggested by the authors, we use $J = 3$ different processes. We used the coefficients $\gamma, \epsilon, \mu_{MB}$ which have been extracted from the NOVAREF data set [26] that consists of high-resolution demand profiles for 12 German households. Extracting the coefficients from a data set with more consumers would be desirable. Still, to our knowledge, there is no publicly available data set with a sufficient time resolution. Fig 3 shows two illustrative, realistic demand time series.

3 Results

3.1 Analytic baseline

To assess the performance of the tuned system, we define a baseline derived from analytic considerations. The goal is to find a relation between the parameters of the system and the specification, which brings both dynamics as close to each other as possible. This is an intricate task as the dynamics of the N5 are non-linear and multi-dimensional. The calculations only consider the asymptotic state of the system, as including the transient behaviors is not

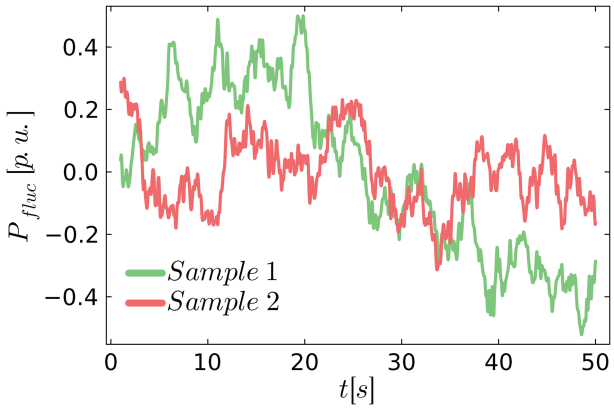


Fig 3. Two realizations of the realistic demand fluctuations.

https://doi.org/10.1371/journal.pone.0322328.g003

analytically tractable. In the following, we present the simplifications made for the calculations and the main steps to arrive at the baselines. The full derivation can be found in the S1 Appendix.

Simplification 1. *All buses are modeled as swing equations with controlled power generation, as in Eq (5).*

All buses rotate at the nominal, synchronous frequency $\omega_0 = 0$ during normal operation. Due to the proportional term, the frequency asymptotically reaches a synchronous state ω^* after a power jump. The synchronous state may not equal the nominal frequency ω_0. The asymptotic frequency ω^* depends on the asymptotic control action u^*. Therefore, we find different results for ω^* for each controller.

Simplification 2. *Wind plants and hydro machines perfectly follow the reference power P_{ref}, meaning that $P_{m,i} = P_{ref,i}$.*

Simplification 3. *The control design and the control parameters of the system are homogeneous.*

This means that the control and respective parameters are equal across all buses, e.g., $D_i = D_{sys}$ for all buses i. The same holds for the other control parameters K_i, T_i, G_i.

The inertia constants H_i, which determine the initial response, are given for the N5 system and can not be controlled as they are physical properties of the machines. The specification inertia has been chosen such that $\sum H_{i,sys} = H_{spec}$, ensuring the same initial frequency response under our simplifications.

For the P-controller, there is no additional control, i.e., $u = 0$, which results in the following equation for the asymptotic frequency ω^*:

$$\omega^* = \frac{\Delta P_{total}}{MD_{sys}} \tag{13}$$

where M is the total number of buses, we define the total power mismatch as ΔP_{total} as the sum of all power mismatches at the buses: $\Delta P_{total} = \sum_i^M P_{ref,i}. - P_{e,i}.$ The total power mismatch ΔP_{total} is the same for the system and specification. Hence, we find $D_{base} = MD_{sys}$ as the baseline.

For the PI controller, it is known that the asymptotic error, in our case the asymptotic frequency ω^*, always reaches zero. We find the following relation for the asymptotic frequency ω^*:

$$\omega^* = 0 = \frac{\Delta P_{total} - K_{sys} \sum_i \int_0^\infty \omega_i(t)}{MD_{sys}}, \tag{14}$$

thus the baseline integral gain becomes $K_{base} = MK_{sys}$.

For the PLI controller, we find the asymptotic control action:

$$u^* = \frac{\omega^*}{G_{sys}}. \tag{15}$$

Using the asymptotic control action u^*, we find the asymptotic frequency:

$$\omega^* = \frac{\Delta P_{total}}{MD_{sys} - M(1/G_{sys})}. \tag{16}$$

Hence, $G_{base} = G_{sys}/M$ has to be chosen such that the system and specification end up in the same asymptotic state. We can not define a baseline for the time constant T as it neither influences the asymptotic state nor the initial response of the system.

In addition to serving as a baseline, the analytic considerations are vital for the optimization. The parameter space is multidimensional, and its landscape is unknown. Thus, it is crucial to start from a good initial guess that is already close to the global minima to avoid excessive computation times or convergence into local minima.

3.2 Numerical results

3.2.1 Random modes. As a first step, we benchmarked the simulation times of both the specification and the system to show the possible speed-up. The benchmark shows that the specification runs significantly faster than the system across all control designs. A relative speed-up ranging from approximately 6.42 to 6.83 times can be achieved for one sample. More details on the benchmark can be found in the S1 Appendix and in the S1 Table.

The following shows the results of applying ProBeTune to the N5 system. Fig 4 illustrates the behavioral distance d^{ρ} between the system and the specification at different stages in the tuning pipeline for the three control strategies. Exact values for the distances are provided in the S3 Table. Fig 4 shows that the baseline performance o_{base} shows substantial deviations from the desired behavior, with all controllers exhibiting similar deviation levels.

The initial distances d^{ρ}_{init}, calculated using Eq (3), are significantly better than the baseline performance. This is expected due to the simplifications, especially since only the asymptotic behavior is considered for the baseline. The initial distances d^{ρ}_{init} exhibit varying degrees of misalignment, with the PI strategy having the least deviation, while the P and PLI controllers show higher deviations. It is unclear why this is the case, and we will see in the next section that this behavior does not persist for different fluctuations. Investigating why the same control strategies are further from the specification for one stochastic process ρ but not another is left to future investigation.

After the tuning process, the distances d^{ρ}_{end} are significantly reduced across all controllers in the same order of magnitude. As expected, including the controllable parameters of the N5 in the optimization further reduces the behavioral distance. Further, the system parameters p_{opt} after tuning are inhomogeneous, meaning that they are specialized for each bus, unlike

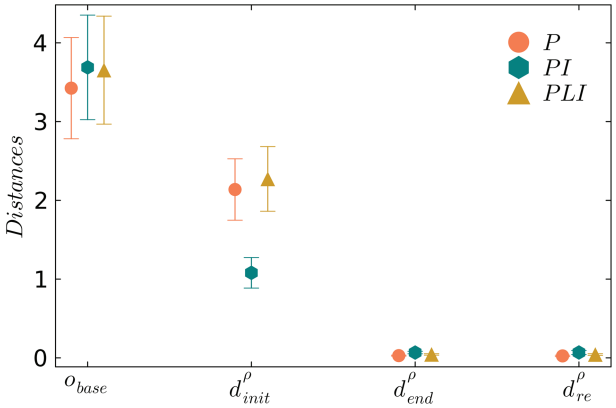


Fig 4. Comparison between the behavioral distances at the different steps in the tuning pipeline for the random mode fluctuations.

https://doi.org/10.1371/journal.pone.0322328.g004

for the initial distance d^{ρ}_{init} where homogeneous system control parameters are employed, see Sect 3.1.

Notably, the distances after resampling, d^{ρ}_{re}, are identical to d^{ρ}_{end}, indicating that no overfitting has occurred and the system has accurately learned the behavior of the specification. These results demonstrate the effectiveness of the behavioral distance approach in combination with tuning.

To better visualize different levels of behavioral distances, we plot exemplary trajectories before and after the tuning process. Figs 5–7 show the frequency f of the specification and the PCC before and after tuning for various scenarios of demand fluctuations. In the pre-tuned state, indicated by the behavioral distance d^{ρ}_{init}, the specification and the system exhibit similar reactions to the demand fluctuations, showing the same peaks. However, the shape and amplitudes of these peaks are not well matched. In the tuned state, we observe a close alignment between the shapes and amplitudes of the peaks for all controllers, as anticipated from the small behavioral distances. This further visualizes the effectiveness of the tuning process.

3.2.2 Realistic demand fluctuations. We have also performed a benchmark for the system and specification for the realistic demand fluctuations. The specification runs significantly faster than the system across all control designs, with a relative speed-up ranging from approximately 18.69 to 22.62 times for a single sample. Further details can be found in the S1 Appendix and in the S2 Table.

As in the previous section, we analyze the behavioral distances over the different steps in the tuning pipeline. Fig 8 represents behavioral distance for the realistic demand fluctuations, and the exact values are given in S4 Table. In Fig 8, we can again see that the baseline o_{base} showcases significant deviations between the system and the desired specification behavior. We can also see that the PI and PLI controllers show more significant deviations than the P controller. As in the previous example, we can see that the initial distances d^{ρ}_{init} are

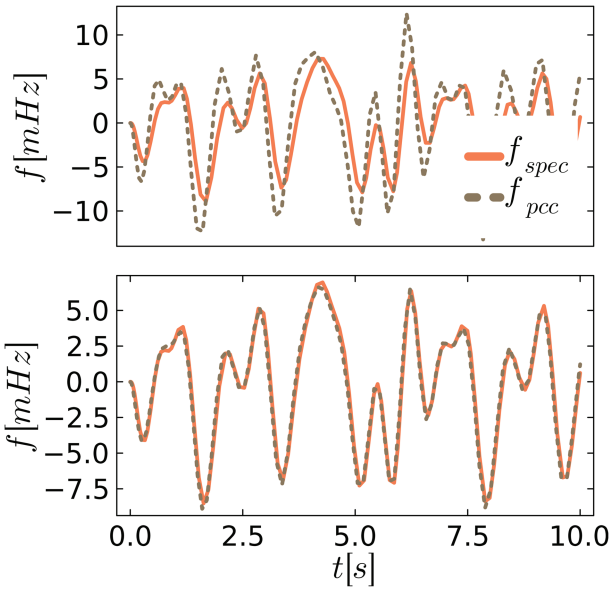


Fig 5. Comparison between the system and the specification behavior for P control. The upper figures always show system and specification at the initial distance d^{ρ}_{init}, and the lower figure shows them at the distance d^{ρ}_{end} after tuning.

https://doi.org/10.1371/journal.pone.0322328.g005

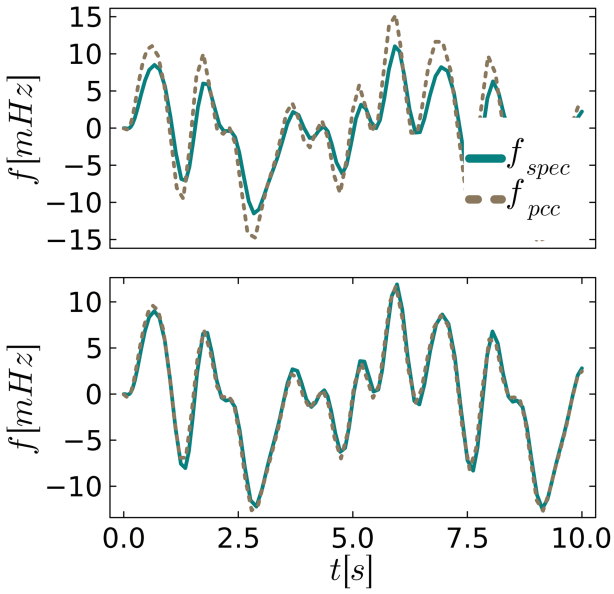


Fig 6. Comparison between the system and the specification behavior for PI control. The upper figures always show system and specification at the initial distance d^{ρ}_{init}, and the lower figure shows them at the distance d^{ρ}_{end} after tuning.

https://doi.org/10.1371/journal.pone.0322328.g006

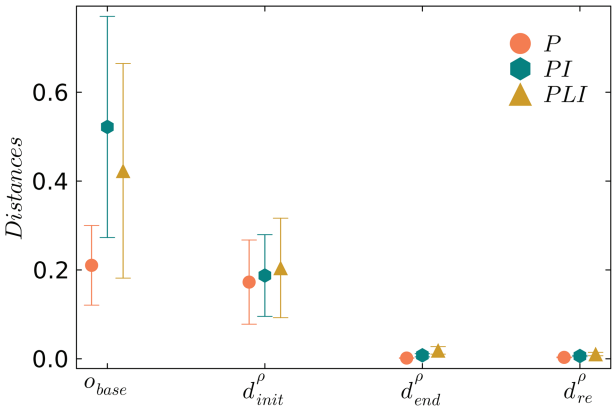


Fig 7. Comparison between the system and the specification behavior for PLI control. The upper figures always show system and specification at the initial distance d^{ρ}_{init}, and the lower figure shows them at the distance d^{ρ}_{end} after tuning.

https://doi.org/10.1371/journal.pone.0322328.g007

significantly lower than the baselines for all controllers. We can especially see an improvement in the PI controller. After tuning, the distances d^{ρ}_{end} are significantly reduced across all controllers as in the previous example. The resampled distances d^{ρ}_{re} match d^{ρ}_{end}, which confirms that no over-fitting has occurred and the system has effectively learned the specified behavior. These results again highlight the success of the tuning processes and the ProBeTune framework overall.

In Figs 9–11 we again visualize exemplary trajectories of the untuned and tuned system and specification. A close match between the system and specification is observed for all controllers in the tuned state, consistent with the small behavioral distances.

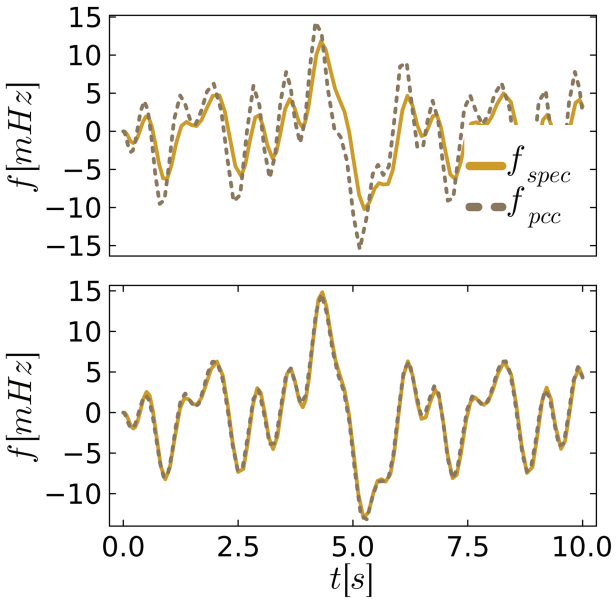


Fig 8. Comparison between the behavioral distances at the different steps in the tuning pipeline for the realistic demand fluctuations.

https://doi.org/10.1371/journal.pone.0322328.g008

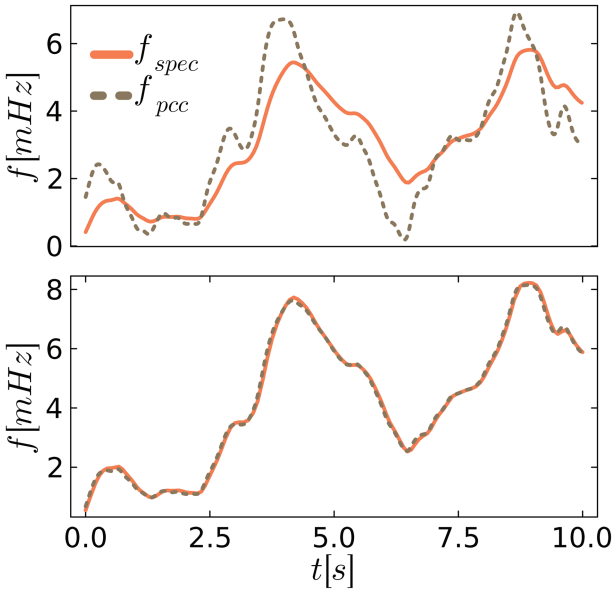


Fig 9. Comparison between the system and the specification for P control. The upper figures show the system and specification at the initial distance d^{ρ}_{init}, and the lower figure shows them at the distance d^{ρ}_{end} after tuning.

https://doi.org/10.1371/journal.pone.0322328.g009

4 Discussion

In this paper, we have applied the novel ProBeTune concept [8] to realistic power grid dynamics for the first time. ProBeTune is a probabilistic, behavioral strategy to reduce the complexity of networked systems by reducing it to a much simpler specification. The reduction is achieved by introducing the behavioral distance, a measure that specifies the difference

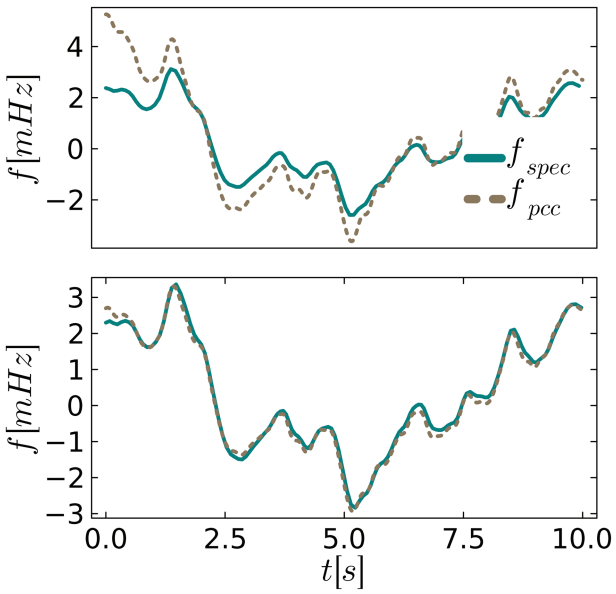


Fig 10. Comparison between the system and the specification for PI control. The upper figures show the system and specification at the initial distance d°_{init}, and the lower figure shows them at the distance d°_{end} after tuning.

https://doi.org/10.1371/journal.pone.0322328.g010

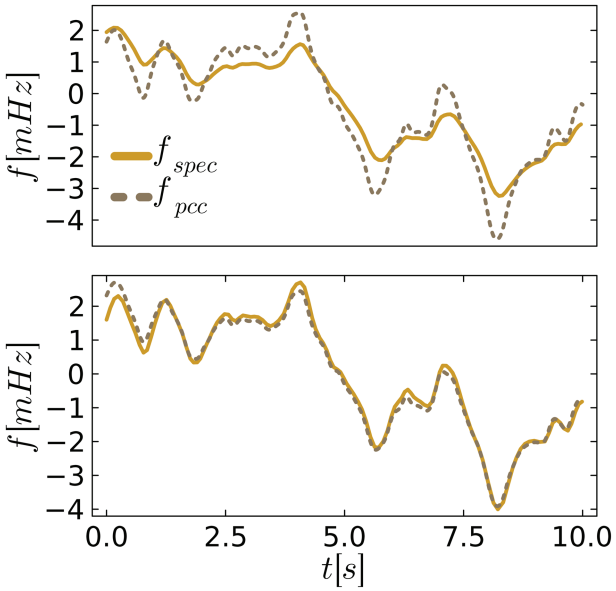


Fig 11. Comparison between the system and the specification for PLI control. The upper figures show the system and specification at the initial distance d°_{init}, and the lower figure shows them at the distance d°_{end} after tuning.

https://doi.org/10.1371/journal.pone.0322328.g011

between the dynamics of two systems, and then minimizing this distance. The N5 system [9] has been used as the test case.

As an initial step, we analytically determined baseline control parameters to align the system's dynamics with the specification. We have shown that behavioral distance applies to power grids and that this distance can be effectively optimized. The behavioral distance has

been successfully reduced by orders of magnitude for all experiments. The results of this study show that the swing equation with appropriate controllers and parameter choices is an excellent and efficient model that can aggregate parts of the power grid. This has been demonstrated by using different controllers and various scenarios. Depending on the configuration, a simulation speed-up of 6.42 up to 22.62 times can be achieved by replacing the system with the specification.

These results are particularly interesting for understanding the dynamics of large interconnected systems, which will consist of many microgrids in the future. These lower-level micro-grids are less well understood than transmission systems, and detailed models are scarce, e.g., the demands of households are hard to predict. These lower-level grids will be characterized by high complexity due to the stochastic nature of renewable energy production and demand and the high number of consumers and producers. An aggregation using ProBeTune is helpful so that the individual sub-grids can still be considered in interconnected power grid models. The results presented in this paper lay the foundation for future research in this direction.

Supporting information

S1 Appendix. Implementation details and derivation of the analytical baseline.
(PDF)

S1 Fig. Block diagram hydro.
(PNG)

S2 Fig. Block diagram thermal.
(PNG)

S3 Fig. Block diagram wind.
(PNG)

S1 Table. Comparison of the simulation times for the system and specification using random mode fluctuations.
(PDF)

S2 Table. Comparison of the simulation times for the system and specification using realistic demand fluctuations.
(PDF)

S3 Table. Behavioral distance d^{ρ} between system and specification at the different steps in the tuning pipeline (mode fluctuations).
(PDF)

S4 Table. Behavioral distance d^{ρ} between system and specification at the different steps in the tuning pipeline (realistic fluctuations).
(PDF)

Author contributions

Conceptualization: Anna Büttner, Frank Hellmann.

Formal analysis: Anna Büttner.

Software: Anna Büttner.

Supervision: Frank Hellmann.

Writing – original draft: Anna Büttner, Frank Hellmann.

Writing – review & editing: Anna Büttner, Frank Hellmann.

References

1. Milano F. Power system modelling and scripting. Berlin, Heidelberg: Springer; 2010. https://doi.org/10.1007/978-3-642-13669-6
2. RG-CE System Protection & Dynamics Sub Group. SPD DSA Task Force Dynamic Security Assessment (DSA). European Network of Transmission System Operators for Electricity; 2017.
3. Veramyeva V. All continental Europe and Nordic TSOs' proposal for assumptions and a cost benefit analysis methodology in accordance with article 156(11) of the commission regulation (EU) 2017/1485 of 2 August 2017 establishing a guideline on electricity transmission system operation. 2018. https://eepublicdownloads.entsoe.eu/clean-documents/nc-tasks/EBGL/SOGL_156.11_CBA
4. Milano F, Dörfler F, Hug G, Hill DJ, Verbic G. Foundations and challenges of low-inertia systems (Invited Paper). In: 2018 Power Systems Computation Conference (PSCC). Dublin: IEEE; 2018. p. 1–25.
5. Ackermann T, Andersson G, Söder L. Distributed generation: a definition. Electric Power Syst Res. 2001;57(3):195–204. https://doi.org/10.1016/s0378-7796(01)00101-8
6. Engeland K, Borga M, Creutin J-D, François B, Ramos M-H, Vidal J-P. Space-time variability of climate variables and intermittent renewable electricity production – a review. Renew Sustain Energy Rev. 2017;79:600–17. https://doi.org/10.1016/j.rser.2017.05.046
7. Ghosh S, Senroy N. Balanced truncation approach to power system model order reduction. Electric Power Compon Syst. 2013;41(8):747–64. https://doi.org/10.1080/15325008.2013.769031
8. Hellmann F, Zolotarevskaia E, Kurths J, Raisch J. Probabilistic behavioral distance and tuning—reducing and aggregating complex systems. J Phys Complex. 2023;4(2):025007. https://doi.org/10.1088/2632-072x/acccc9
9. Björk J, Johansson KH, Dörfler F. Dynamic virtual power plant design for fast frequency reserves: coordinating hydro and wind. IEEE Trans Control Netw Syst. 2023;10(3):1266–78. https://doi.org/10.1109/tcns.2022.3181553
10. Machowski J, Bialek JW, Bumby JR. Power system dynamics. 2nd ed. Wiley; 2008.
11. Schmietendorf K, Peinke J, Friedrich R, Kamps O. Self-organized synchronization and voltage stability in networks of synchronous machines. Eur Phys J Spec Top. 2014;223(12):2577–92. https://doi.org/10.1140/epjst/e2014-02209-8
12. Anderson PM, Fouad AA. Power system control and stability. 2nd ed. Piscataway, NJ: IEEE Press; 2003.
13. Rodrigues FA, Peron TKDM, Ji P, Kurths J. The Kuramoto model in complex networks. Phys Rep. 2016;610:1–98. https://doi.org/10.1016/j.physrep.2015.10.008
14. Working Group Prime Mover and Energy Supply. Hydraulic turbine and turbine control models for system dynamic studies. IEEE Trans Power Syst. 1992;7(1):167–79. https://doi.org/10.1109/59.141700
15. Kundur PS. Power system stability. 3rd ed. CRC Press; 2012.
16. Bjork J, Pombo D, Johansson KH. Variable-speed wind turbine control designed for coordinated fast frequency reserves. IEEE Trans Power Syst. 2022;37(2):1471–81. https://doi.org/10.1109/tpwrs.2021.3104905
17. The behavioral approach to open and interconnected systems. IEEE Control Syst. 2007;27(6):46–99. https://doi.org/10.1109/mcs.2007.906923
18. Haberle V, Fisher MW, Prieto-Araujo E, Dorfler F. Control design of dynamic virtual power plants: an adaptive divide-and-conquer approach. IEEE Trans Power Syst. 2022;37(5):4040–53. https://doi.org/10.1109/tpwrs.2021.3139775
19. Häberle V, Tayyebi A, He X, Prieto-Araujo E, Dörfler F. Grid-forming and spatially distributed control design of dynamic virtual power plants. IEEE Trans Smart Grid. 2024;15(2):1761–77. https://doi.org/10.1109/tsg.2023.3311481
20. Weitenberg E, Jiang Y, Zhao C, Mallada E, De Persis C, Dörfler F. Robust decentralized secondary frequency control in power systems: merits and tradeoffs. IEEE Trans Automat Contr. 2019;64(10):3967–82. https://doi.org/10.1109/tac.2018.2884650
21. Dörfler F, Bullo F. Synchronization and transient stability in power networks and nonuniform kuramoto oscillators. SIAM J Control Optim. 2012;50(3):1616–42. https://doi.org/10.1137/110851584

22. Schmietendorf K, Peinke J, Kamps O. The impact of turbulent renewable energy production on power grid stability and quality. Eur Phys J B. 2017;90(11). https://doi.org/10.1140/epjb/e2017-80352-8

23. Anvari M, Werther B, Lohmann G, Wächter M, Peinke J, Beck H-P. Suppressing power output fluctuations of photovoltaic power plants. Solar Energy. 2017;157:735–43. https://doi.org/10.1016/j.solener.2017.08.038

24. Filip S, Javeed A, Trefethen LN. Smooth random functions, random ODEs, and Gaussian processes. SIAM Rev. 2019;61(1):185–205. https://doi.org/10.1137/17m1161853

25. Anvari M, Proedrou E, Schäfer B, Beck C, Kantz H, Timme M. Data-driven load profiles and the dynamics of residential electricity consumption. Nat Commun. 2022;13(1):4593. https://doi.org/10.1038/s41467-022-31942-9 PMID: 35933555

26. Lange M. Novaref, Erstellung neuer Referenzlastprofile zur Auslegung, Dimensionierung und Wirtschaftlichkeitsberechnung von Hausenergieversorgungssystemen. Next Energy; 2016.